Vol. 44 No. 5 (2023)

Performance Analysis of Learning for Gastric Cancer Prediction from Endoscopic Images

[1]Dr T Velumani

[1]Assistant Professor Department of Computer Science Rathinam College of Arts and Science, Coimbatore-21

Abstract: In terms of mortality rates, gastric cancer is second only to lung cancer. Manual gastric slice pathology examination is labor-intensive and prone to observer bias. Endoscopy of the upper digestive tract is commonly used for the screening of gastric cancer. An object identification model, a kind of deep learning, was presented as a means of automating the diagnosis of early stomach cancer using endoscopic pictures. However, difficulties were encountered while attempting to reduce the sum of false positives in the identified findings. Tumour segmentation from the preprocessed pictures was carried out in this study, which is often more challenging and crucial. The research suggests a productive approach that makes use of multi-scale parallel convolution blocks (MPCs). Multi-scale parallel convolutions (MPCs) use filters of variable sizes to extract characteristics that are relevant across a range of tumour sizes. To further aid feature extraction with fewer parameters, residual connections and residual blocks can be used. In addition, the suggested study uses an Artificial plant optimisation algorithm (APOA) to fine-tune the segmentation model's parameters without resorting to post-processing approaches. Finally, gastric cancer detection from endoscopic pictures is accomplished using a hybrid classification strategy that incorporates Convolutional Neural Network (CNN) and Recurrent Neural Network (RNN). Experiments employing 1208 photos from healthy people and 533 photographs from patients with stomach cancer examined detection performance using the 5-fold crossvalidation approach. These findings show promise for the suggested method's application in automated early stomach cancer diagnosis using endoscopic images.

Keywords—Gastric cancer, Multi-scale parallel convolution blocks, Artificial plant optimization algorithm, Convolutional Neural Network, Recurrent Neural Network, Endoscopic images.

1. Introduction

Cancer of the stomach is referred to as gastric cancer. The epithelial cells lining the mucosa are the source of the first cancerous cells. Adenocarcinoma [1] is the most prevalent pathological subtype. Infection with Helicobacter pylori, hereditary and environmental factors, and clinical symptoms such dyspepsia, epigastric pain, and anaemia are common causes [2]. In terms of cancer-related mortality, gastric cancer ranks third globally and second in China. Over a million new instances of stomach cancer are identified each year across the globe [3]. Gastric specimens must be histopathologically evaluated for clinical care, which is a time-consuming process that requires skilled pathologists. However, pathologists are in low supply across the world. There are reportedly not enough pathologists to treat patients in several African nations [4], while China's shortfall is estimated at 90,000. The ageing pathology workforce is an issue in Western nations as well. When it comes to mortality rates, gastric cancer is second only to lung cancer [5]. Since correct preoperative breast cancer staging can lead to more effective clinical practise and better patient outcomes, it is vitally important [6]. Endoscopic ultrasonography, are all ways to stage stomach cancer before surgery. However, patient acceptability is low [7] because to the operation's intricacy, substantial stress to patients, and strong ionising radiation. The non-invasive, operable, handy, and stable nature of endoscopy images (EI) has led to their widespread usage for preoperative stomach cancer staging [8]. By analysing the pixel intensity in the image, texture analysis of EI images can detect subtle differences not visible to the naked eye and deliver quantitative info about tumour heterogeneity, thereby enhancing the value of examination [9, 10].

In fresh years, deep learning has made constant advancements in image processing, thanks to the fast expansion of computer technology. Medical pictures have a high degree of structure, making them amenable to processing by deep learning techniques [11]. Deep learning has been explored widely and intensively for its potential diagnosis accuracy, which has risen to above 95% [12] in the domains of breast cancer, prostate cancer, and brain disorders. Automatic tissue extraction from pathology slides replaces time-consuming and laborious

ISSN: 1001-4055 Vol. 44 No. 5 (2023)

manual tissue extraction, and it may be used even by those without training in cancer tissue identification. Recently, texture analysis has been applied to the evaluation of stomach tumours or lesions, with promising results for predicting gastric cancer's histopathological stage [13]. However, texture analysis has not yet been implemented in the preoperative staging of stomach cancer. Thus, the drive of this paper is to investigate the use of EI texture investigation throughout the spectrum of stomach cancer staging.

Gastric cancer in preprocessed EI pictures is the subject of this study's segmentation and classification efforts. The APOA model is first utilised to find the appropriate hyper-parameter tuning for the MPCs and residual block, which is then used for segmentation. Finally, stomach cancer detection employs the hybrid classifier. The rest of the study is broken down as follows: Section 2 gives an impression of the pertinent literature, Section 3 gives a concise description of the suggested perfect, Section 4 describes the experiments, and Section 5 summarizes the findings.

2. RELATED WORKS

Whole slide images (WSIs) of human stomach cancer tissue sections are used in the proposed multi-task deep learning-based system by Hu et al. [14]. Using a gastric cancer segmentation model, a neural detection perfect, and a PNI decision-making unit, the proposed framework is able to successfully segment the stomach cancer region while also recognising PNI. Our GC-PNI dataset for gastric cancer underwent sufficient comparison studies. Our experimental results reveal that our suggested model has a high sensitivity of 0.972 and a specificity of 0.933 for diagnosing PNI, demonstrating its potential usefulness in practise.

Using deep learning algorithms, Wei et al. [15] have screened patients who would benefit from immunotherapy by predicting critical molecular characteristics in haematoxylin and eosin-stained pictures. To provide additional verification, an external data collection consisting of Asian patients with stomach cancer was incorporated. Additionally, the cellular makeup of tumour stroma was quantified using a segmentation model (HoVer-Net). Area under the curve (AUC) was used to assess the efficacy of the model. The internal an AUC of 0.9386 for the tumour extraction model, whereas the exterior test set yielded an AUC of 0.9062. The AUC for predicting immunotherapy-responsive subtypes is 0.8685 to 0.9461; for predicting genetic alterations it is 0.8283 to 0.9225; and for predicting pathway activity it is 0.7568 to 0.8612. AUCs of 0.7906 and 0.6384 were obtained for predicting status, respectively, in external validation. Some immunotherapy-sensitive subtypes were shown to have a disproportionately large number of inflammatory cells and connective cells, as determined by the segmentation model. The models trained with deep learning show promise as a useful tool for identifying who will benefit most from immunotherapy for stomach cancer.

Using deep learning (DL) methods, Ma et al. [16] offer an autonomous approach for diagnosing early gastric cancer (EGC). This work specifically constructs different DL architectures to realise the automated interpretation of EGC pictures using a fresh annotated endoscopic image dataset obtained from a single-center. In particular, a ResNet-50-derived guided-attention deep network was established for precise score prediction of EGC and feature extraction. To further estimate problematic zones, we integrated a lightweight attention module and multi-scale feature extractor with U-Net. The experimental results on the presented dataset revealed for assignments.

Kim et al. [17] have looked at how AI imaging may help in diagnosing and staging stomach cancer, demonstrating how it can improve patient care. We also investigated the feasibility of using artificial intelligence body morphometry for measuring the clinical effects of gastrectomy. This use of AI shows great potential for analysing postoperative alterations and improving patient outcomes. We also take a look at how far forward artificial intelligence approaches are in their ability to predict outcomes for people with stomach cancer. These prognostic models use AI algorithms to forecast patients' chances of survival and provide crucial data for treating professionals. However, there are restrictions on the use of AI methods for imaging stomach cancer. We anticipate that as AI develops further, we will see state-of-the-art technology adopted into standard clinical practise, ultimately leading to better patient care and results in the ongoing battle against stomach cancer.

Based on mechanism, Guo et al. [18] offer a compact microfuzzy pathology detection algorithm; the YOLOv5 is enhanced under compact and micro fuzzy scenarios of cancer cell detection throughout the breadth of digital pathology; this method is evaluated on the stomach cancer slice dataset. According to the distribution, the network architecture is upgraded, as is the capability to learn features on tiny and microtargets. Shifts in the

concentration and dispersion of networked attention across space and time. Test results reveal an F1_score of 0.616 and a mAP of 0.611 for the deep blur scenario, indicating that it can serve as a decision support for clinical judgement.

For predicting EBVaGC from histology, Zheng et al. [19] present EBVNet, a deep network, and its fusion with pathologists. An internal cross-validation of the EBVNet produces an AUROC of 0.969, an external dataset from different institutes produces an AUROC of 0.941, and The Cancer dataset produces an AUROC of 0.895. Both the EBVNet and the pathologist benefit much from the human-machine merger in terms of diagnosis accuracy. Based on these results, we hypothesise that our EBVNet might offer a novel method for detecting EBVaGC, which could aid in the appropriate selection of gastric cancer patients for immunotherapy.

3. PROPOSED SYSTEM

This research paper tourist attractions the importance of accurate classification of heart disease.

A. Image Dataset

This research made use of the same picture dataset as our earlier work. Our prior research [20] contains patient information and other relevant data. Between July 16, 2013, and August 30, 2017, data from preoperative exams at Fujita Health University Hospital for 42 healthy of GC were obtained for this investigation.

In total, there were 1208 photos in the first category and 533 in the second. In the event that a lesion was discovered, numerous endoscopic pictures were taken from different angles. Gastric cancer patients and lesions are described in Table 1 [20]. Concerning the healthy participants, we reevaluated the situations in which endoscopists had found no abnormalities. Without the presence of a tumour, polyps, or gastritis and the presence of a consistent pattern of assembling mucosa, we classified the mucosa as "healthy" [21].

Features	Number of Cases
Tumor position	
Inferior third	33
Central third	52
Higher third	9
Macroscopic organization	
Type 0-1	0
Type 0-2a	10
Type 0-2b	0
Type 0-2c	63
Type 0-3	0
Type 0 mixed (0-2a+2c)	21
Complexity of tumor invasion	
T1a	71
T1b	23
Histopathological classification	
Undifferentiated	13
Distinguished	75
Varied	6

TABLE 1: CLINICAL FEATURES OF GASTRIC CANCER IN THE DATASET.

B. Data Augmentation

Since the endoscope can take pictures of the stomach from different angles, we can prove that it is rotation- and inversion-invariant. This means that by just rotating and flipping the collected photographs, a wide variety of new images may be made. In this research, we used the original photos for training and then rotated and flipped them for data augmentation to guarantee consistent deep learning performance. To ensure that there were an equal number of GC and healthy patient photos, we produced them using our own programme at 6 and 10 rotation pitch, respectively [20].

ISSN: 1001-4055 Vol. 44 No. 5 (2023)

C. Segmentation

The suggested innovative segmentation architecture for effective stomach cancer segmentation. Each of these routes uses a combination of Res blocks and multi-threaded convolution blocks (MPCs).

Down-Sampling Layers

Starting with an input picture of size 256 256 1, the down-sampling method employs a multi-scale parallel convolution block (MPC) before moving on to a Res block and a max-pooling operation of size 2 2. Equation (1) describes this procedure:

$$y_{kw}^i = \max_{0 \le a} (x i_{k \times n+a} w_{k \times n+b})$$

 $y_{k,w}^i = \max_{0 \le a,b \le p} (x i_{k \times p + a,w \times p + b})$ In Equation (1), a neuron $y_{k,w}^i$ is contemporary on a site (k, w) at the ith output of the down layer. In the ith input map x_i , a neuron $y_{k,w}^i$ is allocated with a extreme value in region $p \times p$.

Multi-Scale Parallel Convolution Blocks (MPCs): The MPC is constructed by a series of parallel convolutions using 1, 3, and 5 by 5 pixel filters with ReLu activations described by the following equation:

$$f(x) = \{x \text{ if } x > 0 \text{ otherwise } 0\}$$

The input to the Res block is the sum of the outputs from the parallel convolutions. MPCs are a powerful extract property from tumours of varied sizes using parallel convolutions. Except for the first MPC, subsequent max-pool actions trigger the MPC. The feature maps for numerous convolutions may be calculated with Equation (3)..

$$g[x,y] = (m*n)[x,y] = \sum_{f} \sum_{h} n[f,h] f[x-f,y-h]$$

The input picture is symbolised by m in the preceding Equation (3), while the kernel or filter is denoted by n. x and y are the matrix, correspondingly.

Res Blocks: A Res block takes the MPC's previous output as its input. The Res block's design begins with a 1 1 convolution, which takes as input N distinct components and outputs N new elements at random locations in the map. The ith input position contains the element value x_i. Similarly, the jth output channel's location is denoted by the value x_j at the appropriate output position. w_ij is the weight matrix among formulation:

$$x_i = \left(\sum_{i}^{N} w_{ij} * x_i\right) + b_j$$

As a projection layer, these 1 1 convolutions reduce the number of filters or last layer while increasing them in the early layer. The shortcut used here is determined by the following equation:

$$y = F(x, \{W_i\} + x)$$

The input and output layer vectors are characterized by x and y. A residual charting that is to be learned is characterized by the term $F(x,\{W_i\})$. In our Res blocks, layers $F=W_2\sigma(W_1x)$, in of where s is a illustration of the ReLu activation function. As a result, we can calculate a F+x operation by using an addition and a short-cut connection. This convenient link does not change the network equation by adding a new parameter (Equation 4). If the dimensions of F and x are the done. In the event that the dimensions are not equal, the linear projection is carried out using the shortcut connection. Ws stands for the linear projection, which is calculated using Eq. (6).

$$y = F(x, \{W_i\}) + W_s x$$

In order to avoid model overfitting, we repeat our downsampling procedure four times, after which we employ a layer of 0.05. The Res block's output is combined with that of a parallel convolution block. In addition, we use 16, 32, 64, and 128-bit filters in each of our convolution blocks.

- Bottleneck Layer: at our proposed architecture, Res blocks are used at the bottleneck layer following a multi-scale parallel convolution block (MPC). The down-sampling pipeline is sent into the MPC as input. The combined output of its many different-sized filters is sent into the Res block. The bottleneck layers go into the first up-sampling layer, a transposed convolution layer. A feature map with these dimensions (16 x 16 x 256) and 32 filters is sent into the bottleneck layer.
- Up-Sampling Layers: In the up-sampling layers, we employ with a 33 size and a 22 stride. Transposed convolution operates as a deconvolution layer and up-samples pictures with sufficient learning, as opposed to the simple up operation which just doubles the dimension of the input picture without any weights.

Other names for them include fractionally strided convolutions. The convolution may be expressed using a sparse matrix C if we assume that the inputs and outputs zero kernel elements in a sparse matrix C are denoted by W_ij. The transpose of a sparse matrix C, however, may be easily obtained, allowing for a backwards run of the convolution process. The error is multiplied by the transpose of a sparse matrix and then back-propagated. In order to calculate the kernel w for each convolutional iteration, we multiply the sparse matrix C by its transpose, CT. Transposed convolution with kernel w's forward and backward passes are obtained by multiplying the sparse matrix C by (CT)T. Transposed convolutions, skip connections, multi-layer perceptrons, and Res blocks are the upsampling layers' organisational pillars. Each transpose convolution layer has 64 filters, 32 filters, and 16 filters for a grand total of 128 filters. These down sampling layers aid in resizing the feature maps to their original dimensions by contributing more spatial and contextual info to the segmentation image. The context might be transferred from the down-sampling levels to the up-sampling ones using skip connections. The final segmented image has 256x256x1 dimensions and is generated by an 11 convolution followed by a sigmoid activation function.

5) Skip Connections: Some of the finer details in a photograph may be lost if it were down-sampled. Using the skip connections, the down-sampling layers may recover the lost details and reconstruct the original low-level features. The outputs of layers may be concatenated with the inputs of the up-sampling layers to provide the contextual info for localisation. Subsequent the concatenation procedure, a dropout at the same rate is utilised, followed by blocks, and lastly Res blocks with shortcut connections.

D. Hyper-parameter tuning using Artificial Plant Optimization Algorithm (APOA)

An method for solving global optimisation issues is the Artificial Plant Optimisation method (APOA). It's a biologically motivated programme designed to simulate plant development. A plant's APO specifies its optimal growing conditions. The resources in this bounded area are both stable, like air and water, and dynamic, like sunshine. Using operators such as photosynthesis, phototropism, apical dominance, and skototropism, the fitness value of individual plant branches (candidate solutions) is determined. Plants' photosynthesis rates and their phototropic growth patterns may be used to estimate how much energy they produce. Additionally crucial, apical dominance and skototropism further refine the search for a candidate solution on the way to the best option.

1) Photosynthesis Operator: reflects the problem's dimensionality, and 'coeff' is the controllinThe process through which plants create their own energy, known as photosynthesis. The pace at which energy is created during photosynthesis is known as the photosynthetic rate. The quality of the generated energy is obtained along the path of growth using a rectangular hyperbolic model.

$$r_i(t) = \frac{\mu I f_i(t) R_{max}}{\mu I f_i(t) + R_{max}} - D_R$$

where $r_i(t)$ represents ith branch's at time t, μ is the competence of initial quantum, R_{max} is the rate, and D_R signifies the dark breathing rate. μ , R_{max} and R control the size of photosynthetic as 0.055, 30.2, and 1.44, individually [22]. $If_i(t)$ is the intensity of light and is characterised as:

$$If_i(t) = \frac{f_{worst}(t) - f_i(t)}{f_{worst}(t) - f_{best}(t)}$$

where $f_{best}(t)$ and $f_{worst}(t)$ are the best and worst t, correspondingly. $f_i(t)$ is the light strength of branch 'i'.

2) Phototropism Operator: The term "phototropism" describes how plants adjust their development patterns based on the orientation of their light sources. Since higher light intensities result in more energy production, they are favoured in APOA. Therefore, the branches are drawn to these locations. The 'ith' Branches adopt the supplementary framework.:

$$g_i(t+1) = g_i(t) + C_p.F_i(t).rd()$$

where, C_p is a parameter that characterises the rate of energy adaptation and it is used to control the growing scope per unit time. $F_i(t)$ characterises the growing force, rd() is a random amount sampled from a unchanging distribution.

 $F_i(t)$ for ith branch is calculated by:

ISSN: 1001-4055 Vol. 44 No. 5 (2023)

$$F_i(t) = \frac{F_i^{total}}{\|g_i(t) - g_p(t)\|} \cdot (\|g_i(t) - g_p(t)\|)$$

where $\|.\|$ signifies the Euclidean distance. $F_i^{total}(t)$ is intended as:

$$F_i^{total}(t) = \sum_{i \neq p}^{t} coff. e^{-\dim P_i(t)} - e^{-\dim P_p(t)}$$

'dim' 'coeff' stands for the growth direction regulating parameter, while 'd' stands for the problem's dimension.:

$$coeff = \begin{cases} 1 & if \ P_i(t) > P_p(t) \\ -1 & if \ P_i(t) < P_p(t) \\ 0 & otherwise \end{cases}$$

To account for the impact of chance, we have also incorporated a tiny probability, denoted by Pm.:

$$x_i(t+1) = x_{min} + (x_{max} - x_{min}).rd_1(), if (rd_2() < P_m)$$

given two uniformly distributed random integers, rd_1 () and rd_2 (). These statistics are created to provide an element of unpredictability to the occurrences, making them feel more spontaneous, like they would in the real world. As was previously mentioned, the random variables rd_1 () and rd_2 () can take on any value between 0 and 1, where 1 represents an infinitely likely occurrence of the random event Pm.

Apical Dominance and Skototropism Operative: One of APO's defining characteristics is apical dominance. The chief stem of a plant develops more than the other stems, and the main stem branch of a given branch develops more noticeably and dominantly than the other branchlets. The apical bud plays a crucial role in determining the branch's growth direction because apical dominance distinguishes between two types of buds, the apical bud and the lateral bud. When the apical bud generates the auxin IAA (Indole-3-acetic acid), it stunts the development of the lateral buds. Lower levels of IAA in the plants allow the lateral buds to develop and compete for dominance if the apical bud is absent. Since the apical bud's light is higher than that of the lateral buds, APOA considers it to be in the optimal place. A population's optimal state (t) can be interpreted as:

$$g(t) = argmin\{f(x_u(t))|u = 1, ..., n\}$$

Because of its superior growth and efficiency, (t) is the target of the apical dominance operator. In the event that ran() is used to define a random number, then behaviour might vary depending on the parameters..

Condition 1: if $\frac{1}{n} < rand() < rate$, then

$$g_k(t+1) = g_k(t) + (g_k(t) - x_{worst,k(t)}).$$
 growth. r

Where

$$x_{worst,k(t)} = argmax\{f(x_u(t))|u=1,\dots,n\}$$

Condition 2: if $rand() \le \frac{1}{n}$, then

$$g_k(t+1) = L + (U-L).rand_1$$

where L and U are the domain's minimum and maximum values. (t) is meaningless under any other circumstances.

In contrast to phototropism, in which a plant grows towards its light source, skototropism describes the opposite behaviour. Negative phototropism, or skototropism, occurs when plants develop away from the source of light. Roots and certain vine shoots exhibit skototropism, which permits things and aid in the ascent. This is in contrast to the positive phototropism exhibited by most plant shoots.

Vines in tropical woodlands often exhibit skototropism. Although there is a plenty of water and nutrients in the soil, enough sunshine is still a problem for these plants in the vast forests. However, if the vines are seeking sunshine, they will be disappointed if they attempt to grow towards canopy openings. They gravitate towards the shade, such as the trunks and bases of huge trees. This allows them to get traction and ascend lofty trees, where they may finally bask in the sunlight. These vines display phototropism instead of skototropism after they attach to a stable surface.

E. Classification using Hybrid DL

1) **Convolutional Neural Network:** In order to train a CNN, matrices are multiplied to provide inputs for the network. Convolution is the name for this technique. For this reason, we refer to this network as a CNN.

A CNN is trained using the segmented pictures. Training entails setting a kernel size and a few filters. A CNN can have more than one dimension. A Network (Conv1D) is typically used for text categorization and natural language processing. Conv1D processes word vectors stored in one-dimensional arrays. A CNN uses a filter with a fixed-size window to iteratively process the training data, producing an output by multiplying the input by the filter's weights. This output array may be thought of as a feature map or data filter. This method is used to identify a feature in the training data.

The number of feature maps to be employed is supplied as the number of filters, and the size of the filter is stated as the kernel size. CNN may then be used to learn these locally-relevant characteristics from the training data itself.

2) Recurrent Neural Networks: For learning purposes, a RNN uses a sequential processing of data. The fact that it can remember what occurred before the present sequence being treated is evidence in favour of the validity of the sequential approach taken. The output from one time step is fed into the next, thus the name "recurrent." To do this, the result from the prior time step is kept in mind. In turn, this enables us to learn causal relationships in the training data over time. Layers of memory cells make up RNN. RNN may make use of a variety of different kinds of memory cells. Long short-term memory (LSTM) cells are one example. As the sequence is state, LSTM consists of a cell state, a carry, and the current word vector. In a sequential operation, the carry must guarantee that no data is lost.

Weights and three types of gates make up an LSTM cell, which is used in the learning process. Each time step has a set of gates: for ignoring data that is no longer relevant.

3) Hybrid CNN-RNN model: The suggested model leverages both the CNN's and the LSTM's strengths, namely their capacity to dependencies, respectively. To begin, input vectors are run through a Conv1D CNN layer to get at the text-level local features. The RNN layer consisting of LSTM units/cells receives its input from the CNN layer's output (the feature maps). After the CNN has collected local features from the segmented pictures, the RNN layer utilises those features to learn the long-term relationships between the segments and the final classification of gastric cancer or no stomach cancer. Figure 1 depicts the suggested model.

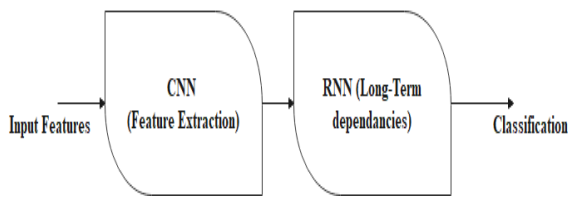


Fig. 1. The proposed hybrid models.

Due to their capacity to capture sequential properties of input data, CNN-RNN combinations have been shown to be successful in a number of classification and regression applications. CNN's prowess with spatial relations allows it to recognise relationships between text entities and crucial characteristics in picture classification tasks, and RNN can learn these features.

4. RESULTS AND DISCUSSION

All tests were conducted on a 3.6 GHz Intel Core i9- with 16 GB of RAM and an NVIDIA GTX 2080Ti graphics dispensation unit. In addition, we use the accelerated computing resources of CUDA10.1 and cuDNN7.6.5 in the deep learning framework Pytorch.

A. Segmentation Evaluation Metrics

These five metrics have the following definitions, where A is the gastric segmentation result and B is the gold standard:

Dice coefficient (DC): the similarity among two sets, having a range of [0,1]. Accurate segmentation is indicated by larger values.

$$Dice(A,B) = \frac{2|A \cap B|}{|A| + |B|}$$

Volume Overlap Error (VOE): volumetric inconsistency amid segmented and raw data.

Vol. 44 No. 5 (2023)

$$VOE(A, B) = 1 - \frac{|A \cap B|}{|A \cup B|}$$

RVD: This statistic determines if the outcome is too fragmented. More accurate segmentation is indicated by values closer to 0.

$$RVD(A,B) = \frac{|B| - |A|}{|A|}$$

$$ASD(A,B) = \frac{1}{|S(A)| + |S(B)|} \left(\sum_{p \in S(A)} d(p,S(B)) + \sum_{q \in S(B)} d(q,S(A)) \right)$$

$$MSD(A,B) = max \left\{ \max_{p \in S(A)} d(p,S(B)), \max_{q \in S(B)} d(p,S(A)) \right\}$$
(21)

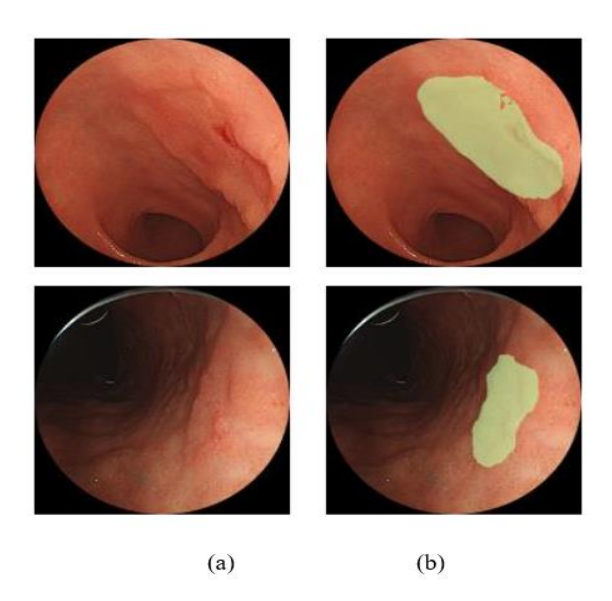


Fig. 2. Segmentation sample images.

Fig. 3.

TABLE 2: THE CONSEQUENCES OF A QUANTITATIVE CONTRAST WITH METHODS ON TRAINING DATASETS.

Models	Dice (%)	RVD (%)	VOE (%)	ASD (mm)	MSD (mm)
FCM	95.60±3.41	-2.38±2.16	8.23±5.89	2.19±0.38	36.69±1.45
K-Means	96.94±1.78	-0.54±2.24	5.31±3.48	1.95±0.34	30.66±2.03
Ostu thresholding	96.66±2.19	-1.29±3.58	6.38±3.93	1.80±0.38	28.30±2.05
Proposed	97.31±1.49	-1.08±2.06	5.37±3.27	1.85±0.30	27.45±1.89

In above Table 2 signifies that the consequences of a quantitative contrast with tactics on Training datasets. In the analysis of FCM model attained the dice value as 95.60 ± 3.41 and the RVD value as -2.38 ± 2.16 and VOE range as 8.23 ± 5.89 and the ASD value as 2.19 ± 0.38 and finally the MSD value as 36.69 ± 1.45 correspondingly. After the K-Means model attained the dice value as 96.94 ± 1.78 - 0.54 ± 2.24 5.31 ± 3.48 1.95 ± 0.34 and finally the MSD value as 30.66 ± 2.03 respectively. After the Ostu thresholding model attained the dice value as 96.66 ± 2.19 and the RVD value as -1.29 ± 3.58 and also RVD range as 6.38 ± 3.93 and VOE range as 1.80 ± 0.38 and finally the MSD value as 28.30 ± 2.05 respectively. After the Proposed model attained the dice value as 97.31 ± 1.49 and the RVD value as -1.08 ± 2.06 and 5.37 ± 3.27 and VOE range as 1.85 ± 0.30 and finally the MSD value as 27.45 ± 1.89 respectively.

B. Classification

Table 3 presents the comparative investigation of projected classifier model.

Metrics	Proposed	RNN	CNN	DBN
TP	27	26	26.25	25
FP	3	5	3.75	5
FN	3	86	3.75	5
TN	87	87	86.25	85
Preci.	90	87	87.75	83.50
Sensi.	90	86.75	87.5	83.25
Speci.	97	95.75	96	94.5
Accuracy	95	87	88	83

TABLE 3: INVESTIGATION OF PROJECTED CLASSIFIER FOR GASTRIC CANCER.

In above Table 3 signifies that the Investigation of Projected Classifier for Gastric Cancer. In the analysis of TP standard of proposed model reached a TP as 27 and also the RNN model reached 26 and then CNN model reached 26.25 and DBN reached 25 correspondingly. Then the FP standard of proposed model reached a TP as 3 and also the RNN model reached 5 and then CNN model reached 3.75 and DBN reached 5 correspondingly. Then the FN standard of proposed model reached a TP as 3 and also the RNN model reached 3.75 and DBN reached 5 correspondingly. Then the TN standard of proposed model reached a TP as 87 and also the RNN model reached 87 and then CNN model reached 86.25 and DBN reached 85 correspondingly. Then the correspondingly. Then the Preci. standard of proposed model reached a TP as 90.87 and also the RNN model reached 87.75 and DBN reached 83.50 correspondingly. Then the Sensi. standard of proposed model reached a TP as 90 and also the RNN model reached 86.75 and the CNN model as87.5 and DBN reached 83.25 correspondingly. Then the Specificity standard of proposed model reached a TP as 97 and also the RNN model reached 95.75 and then CNN model reached 96 and DBN reached 94.5 correspondingly. Then the Accuracy standard of proposed model reached a TP as 95 and also the RNN model reached 87 and then CNN model reached 88 and DBN reached 83 correspondingly.

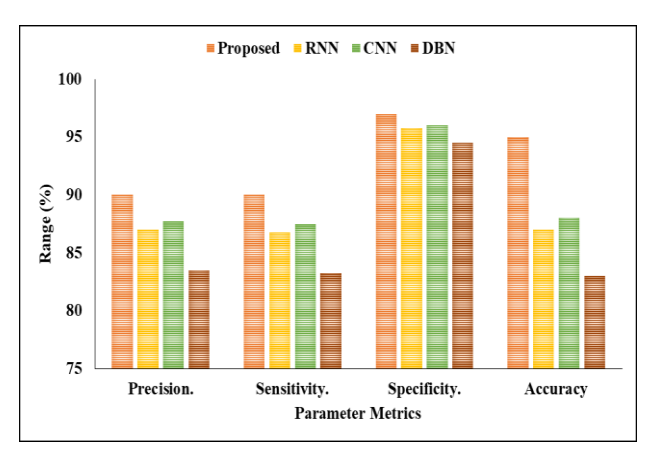


Fig. 4. Graphical Representation of proposed model for different metrics.

5. CONCLUSIONS

This study identified challenges associated with stomach tumour segmentation and proposed a method to overcome them. Many studies have developed two-stage procedures that first segment the tumour from the stomach cancer. This method is laborious and has a greater potential for error. In this study, we presented a method for solving these problems by directly segmenting out the tumour from EI pictures, which is a significant technical challenge. However, it is a comprehensive segmentation method, running quickly and producing reliable results on the provided test data. In order to encode multi-scale characteristics of varying tumour sizes, the suggested method makes use of MPCs. Tumour traits may be encoded using less network parameters thanks

to Res blocks being incorporated into the design. All of these features improve our model's segmentation accuracy. In addition, our method does not necessitate further post-preprocessing actions for the improvement of segmentation outcomes. The APOA model is then utilised to fine-tune the model's parameters, and a hybrid classifier is deployed to make the cancer diagnosis. The new method outperformed prior strategies in an evaluation utilising endoscopic pictures of patients with early-stage GC and healthy controls. These findings demonstrate the efficiency of our strategy for the automated endoscopic identification of early GC. Either an optimisation model for hyper-parameter tweaking or a U-Net with a revised architecture will be included to further enhance the suggested model in the future.

REFERENCES

- [1] N. Kumar, P. Nandihal, M. R. B, P. K. Pareek, N. T and S. S. R, "A Novel Machine Learning-Based Artificial Voice Box," 2022 Second International Conference on Advanced Technologies in Intelligent Control, Environment, Computing & Communication Engineering (ICATIECE), Bangalore, India, 2022, pp. 1-7, doi: 10.1109/ICATIECE56365.2022.10046967.
- [2] P. Nandihal, V. Shetty S, T. Guha and P. K. Pareek, "Glioma Detection using Improved Artificial Neural Network in MRI Images," 2022 IEEE 2nd Mysore Sub Section International Conference (MysuruCon), Mysuru, India, 2022, pp. 1-9, doi: 10.1109/MysuruCon55714.2022.9972712.
- [3] Subbalakshmi, C., Pareek, P.K., Narayana, M.V. (2022). A Gravitational Search Algorithm Study on Text Summarization Using NLP. In: Kumar, A., Fister Jr., I., Gupta, P.K., Debayle, J., Zhang, Z.J., Usman, M. (eds) Artificial Intelligence and Data Science. ICAIDS 2021. Communications in Computer and Information Science, vol 1673. Springer, Cham. https://doi.org/10.1007/978-3-031-21385-4_13
- [4] S. Prasath Alais Surendhar, Govindaraj Ramkumar, Ram Prasad, Piyush Kumar Pareek, R. Subbiah, Abdullah A. Alarfaj, Abdurahman Hajinur Hirad, S. S. Priya, Raja Raju, "Prediction of Escherichia coli Bacterial and Coliforms on Plants through Artificial Neural Network", Advances in Materials Science and Engineering, vol. 2022, Article ID 9793790, 13 pages, 2022. https://doi.org/10.1155/2022/9793790
- [5] M. V. Kumar, G. P. Ramesh, P. K. Pareek, H. A. Deepak and J. A. Babu, "Robotic Attendance Scheme in the Classroom Using Artificial Intelligence and Internet of Things," 2023 International Conference on Applied Intelligence and Sustainable Computing (ICAISC), Dharwad, India, 2023, pp. 1-6, doi: 10.1109/ICAISC58445.2023.10200650.
- [6] S. Kumar, P. K. Pareek, P. Rashmi, R. Deepak and V. Petli, "IoT Based Automated Poultry Farm for Layer Chicken using Artificial Intelligence Techniques," 2023 International Conference on Applied Intelligence and Sustainable Computing (ICAISC), Dharwad, India, 2023, pp. 1-7, doi: 10.1109/ICAISC58445.2023.10199649.
- [7] V. S. Kumar, P. K. Pareek, V. H. Costa de Albuquerque, A. Khanna, D. Gupta and D. R. S, "Multimodal Sentiment Analysis using Speech Signals with Machine Learning Techniques," 2022 IEEE 2nd Mysore Sub Section International Conference (MysuruCon), Mysuru, India, 2022, pp. 1-8, doi: 10.1109/MysuruCon55714.2022.9972662.
- [8] D. S M, R. N, S. K and P. K. Pareek, "Machine Learning based Education System with Sentiment Analysis for Students," 2022 IEEE 2nd Mysore Sub Section International Conference (MysuruCon), Mysuru, India, 2022, pp. 1-6, doi: 10.1109/MysuruCon55714.2022.9972555.
- [9] Piyush K. Pareek, Pixel Level Image Fusion in Moving objection Detection and Tracking with Machine Learning, Journal of Fusion: Practice and Applications, Vol. 2, No. 1, (2020): 42-60 (Doi: https://doi.org/10.54216/FPA.020105) Piyush K. Pareek, Pixel Level Image Fusion in Moving objection Detection and Tracking with Machine Learning, Journal of Fusion: Practice and Applications, Vol. 2, No. 1, (2020): 42-60 (Doi: https://doi.org/10.54216/FPA.020105)
- [10] S. Aruna, A. Saranya, D. Guru Pandi, S. P. Kavya and P. K. Pareek, "Machine Learning Approach for Detecting Liver Tumours in CT images using the Gray Level Co-Occurrence Metrix," 2023 International Conference on Applied Intelligence and Sustainable Computing (ICAISC), Dharwad, India, 2023, pp. 1-5, doi: 10.1109/ICAISC58445.2023.10199347.

[11] S. Sivakumar, S. Saminathan, R. Ranjana, M. Mohan and P. K. Pareek, "Malware Detection Using The Machine Learning Based Modified Partial Swarm Optimization Approach," 2023 International Conference on Applied Intelligence and Sustainable Computing (ICAISC), Dharwad, India, 2023, pp. 1-5, doi: 10.1109/ICAISC58445.2023.10199796.

- [12] R. Haque, P. K. Pareek, M. B. Islam, F. I. Aziz, S. D. Amarth and K. G. Khushbu, "Improving Drug Review Categorization Using Sentiment Analysis and Machine Learning," 2023 International Conference on Data Science and Network Security (ICDSNS), Tiptur, India, 2023, pp. 1-6, doi: 10.1109/ICDSNS58469.2023.10245841.
- [13] Alqahtani, A., Alqahtani, N., Alsulami, A. A., Ojo, S., Shukla, P. K., Pandit, S. V., Pareek, P. K., & khalifa, H. S. (2023). Classifying electroencephalogram signals using an innovative and effective machine learning method based on chaotic elephant herding optimum. Expert Systems, e13383. https://doi.org/10.1111/exsy.13383
- [14] S. Rani, P. Kumar Pareek, J. Kaur, M. Chauhan and P. Bhambri, "Quantum Machine Learning in Healthcare: Developments and Challenges," 2023 IEEE International Conference on Integrated Circuits and Communication Systems (ICICACS), Raichur, India, 2023, pp. 1-7, doi: 10.1109/ICICACS57338.2023.10100075.
- [15] C. Chethana, Piyush Kumar Pareek, "Analysis of Credit Card Fraud Data Using Various Machine Learning Methods", Big Data, Cloud Computing and IoT, Edition1st Edition, First Published 2023, Imprint Chapman and Hall/CRC, Pages14, eBook ISBN 9781003298335
- [16] Ma, L., Su, X., Ma, L., Gao, X., & Sun, M. (2023). Deep learning for classification and localization of early gastric cancer in endoscopic images. Biomedical Signal Processing and Control, 79, 104200.
- [17] Kim, K. W., Huh, J., Urooj, B., Lee, J., Lee, J., Lee, I. S., ... & Ko, Y. (2023). Artificial Intelligence in Gastric Cancer Imaging With Emphasis on Diagnostic Imaging and Body Morphometry. Journal of Gastric Cancer, 23(3), 388.
- [18] Guo, Q., Yu, W., Song, S., Wang, W., Xie, Y., Huang, L., ... & Wang, S. (2023). Pathological Detection of Micro and Fuzzy Gastric Cancer Cells Based on Deep Learning. Computational and Mathematical Methods in Medicine, 2023.
- [19] Zheng, X., Wang, R., Zhang, X., Sun, Y., Zhang, H., Zhao, Z., ... & Cai, M. (2022). A deep learning model and human-machine fusion for prediction of EBV-associated gastric cancer from histopathology. Nature communications, 13(1), 2790.
- [20] Shibata, T.; Teramoto, A.; Yamada, H.; Ohmiya, N.; Saito, K.; Fujita, H. Automated Detection and Segmentation of Early Gastric Cancer from Endoscopic Images Using Mask R-CNN. Appl. Sci. 2020, 10, 3842.
- [21] Yagi, K.; Nakamura, A.; Sekine, A. Characteristic endoscopic and magnified endoscopic findings in the normal stomach without Helicobacter pylori infection. J. Gastroenterol. Hepatol. 2002, 17, 39–45.
- [22] Sharma, P., Choudhary, K., Gupta, K., Chawla, R., Gupta, D., & Sharma, A. (2020). Artificial plant optimization algorithm to detect heart rate & presence of heart disease using machine learning. Artificial intelligence in medicine, 102, 101752.